ISSN 1054-660X, Laser Physics, 2007, Vol. 17, No. 2, pp. 190–197.

Instabilities and Sound Speed of a Bose–Einstein Condensate in the Kronig–Penney Potential

Xi Dong[a, b] and Biao Wu[a, *]

[a] *Institute of Physics, Chinese Academy of Sciences, P. O. Box 603, Beijing, 100080 China*
[b] *Department of Physics, Tsinghua University, Beijing, 100084 China*
*e-mail: bwu@aphy.iphy.ac.cn

Received August 30, 2006

Abstract—We analyze the full set of Bloch wave stationary solutions for a Bose–Einstein condensate in the Kronig–Penney potential. We investigate the Landau instability and dynamical instability of the Bloch states in the lowest Bloch band, including the loop if it appears. The stability phase diagrams are shown to be similar as in the case of the sinusoidal optical lattice potential. We also compute the speed of sound as a function of the potential strength. The trend is shown to be similar to the sinusoidal case, reflecting our general conclusion that, in any one-dimensional periodic potential, the sound speed always falls monotonically with increasing potential strength, no matter whether the atomic interaction is weak or strong. The Kronig–Penney potential, being analytically tractable and hence more advantageous than the sinusoidal potential, therefore serves as a good model for understanding the phenomena of Bose–Einstein condensation.

PACS numbers: 03.75.Hh, 03.75.Kk, 05.30.Jp, 67.40.Db

DOI: 10.1134/S1054660X07020247

1. INTRODUCTION

Bose–Einstein condensates (BECs) in periodic potentials have been the focus of many studies during the past few years. Ever since the first realization of Bose–Einstein condensation of alkali-metal atoms in 1995 [1–3], there have been many intriguing phenomena related to the properties of BECs in periodic potentials, such as superfluidity, dynamical instability [4–11], Josephson oscillations [12, 13], and Landau–Zener tunneling [14–18]. Specifically, it has been found that the interaction between the BEC atoms can deeply affect the band structure and the instabilities of a BEC in a periodic potential [10].

So far, considerations have been primarily focused on BECs in a sinusoidal optical lattice, which is generated in experiments by the interference of two counterpropagating laser beams and is therefore composed of a single Fourier component. However, if more counterpropagating laser beams of frequencies that are multiples of the fundamental are added, more Fourier components would be introduced, and the potential would hence become a lattice of well-separated peaks. In the limit that the width of these peaks becomes much smaller than the lattice period, the potential virtually becomes a Kronig–Penney potential, i.e., a lattice of delta functions. An experimental scheme to create unconventional optical lattices has recently been proposed in [19].

Theoretically, we start by considering the mean field of a BEC trapped in the Kronig–Penney potential, modeled by the Gross–Pitaevskii (GP) equation [20, 21], which is also called the nonlinear Schrödinger equation (NLS) in numerous areas of physics. A full set of Bloch wave stationary solutions for such a BEC has recently been found, and the structure of the Bloch bands has been studied in detail [22]. The Bogoliubov excitations in such a system have also been investigated [24]. In our work, we investigate the Landau instability (which are closely related to superfluidity), the dynamical instability, and the sound speed of a BEC in the Kronig–Penney potential. We show that the mean-field Bloch states of a BEC in the Kronig–Penney potential exhibit not only the same band structure but also the same properties concerning the instabilities and the sound speed as in the case of the sinusoidal potential. Specifically, both the stability phase diagrams and the functional relationship between the sound speed and the potential strength are similar in these two cases. Since the sinusoidal lattice and the Kronig–Penney potential represent two extreme forms of periodic potentials, our results show convincingly that the fundamental properties of a BEC in a periodic potential do not depend on the shape of a lattice potential. As a result, theorists are at liberty to choose the form of a periodic potential for the convenience of their study.

In the case of the sinusoidal potential, the Bloch wave solutions can only be found numerically [10]. In contrast, the Bloch wave solutions to the Kronig–Penney potential can be described by an analytic expression in terms of a Jacobi elliptic function [22]. Therefore, the Kronig–Penney potential offers certain great advantages over the sinusoidal potential as a theoretical model in investigating the properties of a BEC in a periodic potential. The study of BECs in the Kronig–Penney potential therefore becomes highly interesting.

Our paper is organized as follows. In Section 2, we give an overview of the Bloch wave solutions to the time-independent GP equation and the structure of the Bloch bands. In Section 3, we investigate the Landau instability and dynamical instability of the BEC Bloch states in the lowest Bloch band, including the loop if it appears. Our results are summarized in the stability phase diagrams. The speed of sound as a function of the potential strength is computed in Section 4. The sound speed always falls monotonically with increasing potential strength, no matter whether the atomic interaction is weak or strong. This is in accordance with our analytic expression of the sound speed in the weak potential limit of an arbitrary potential. Finally, in Section 5, we summarize the results and discuss their implications.

2. BLOCK WAVES AND BLOCH BANDS IN THE KRONIG–PENNEY POTENTIAL

We consider a BEC in the presence of a one-dimensional Kronig–Penney potential,

$$V(x) = v\sum_{n=-\infty}^{+\infty}\delta(x-nd), \tag{1}$$

in which v characterizes the strength of the potential and d is the spatial period. The BEC system is quasi-one-dimensional in the sense that its motion in the transverse directions is either confined [6] or negligible [23, 25, 26]. Therefore, the BEC dynamics can be described in the mean-field theory by the one-dimensional GP or NLS equation:

$$i\hbar\frac{\partial\Psi(x,t)}{\partial t} = \left(-\frac{\hbar^2}{2m}\frac{\partial^2}{\partial x^2} + c|\Psi(x,t)|^2 + V(x)\right)\Psi(x,t), \tag{2}$$

where $\Psi(x, t)$ is the macroscopic wave function describing the state of the whole BEC, m is the atomic mass, and c is the nonlinear coefficient characterizing the strength of the short-range pairwise interaction between the BEC atoms.

We seek the stationary solutions of the time-dependent GP Eq. (7). These solutions are determined by the stationary condition

$$\Psi(x,t) = e^{-i\mu t/\hbar}\psi(x) \tag{3}$$

and therefore satisfy the time-independent GP equation

$$-\frac{\hbar^2}{2m}\frac{d^2\psi(x)}{dx^2} + c|\psi(x)|^2\psi(x) + V(x)\psi(x) = \mu\psi(x), \tag{4}$$

in which the wave function $\psi(x)$ describes the nonlinear eigenstate and μ, the nonlinear eigenvalue, is usually called the chemical potential. The absolute square of the wave function $\psi(x)$ is called the density function of the BEC atoms and is denoted by $\rho(x)$. The constraint of particle number conservation imposes on the wave function $\psi(x)$ a normalization condition which, as the result of the periodicity of the BEC system, can be written as

$$\int_0^d|\psi(x)|^2dx = \int_0^d\rho(x)dx = n_0d, \tag{5}$$

where n_0 is the average particle number density of the BEC over a period.

For convenience, we usually rewrite Eqs. (1)–(5) in the dimensionless form as

$$V(x) = v\sum_{n=-\infty}^{+\infty}\delta(x-n), \tag{6}$$

$$i\frac{\partial\Psi(x,t)}{\partial t} = \left(-\frac{1}{2}\frac{\partial^2}{\partial x^2} + c|\Psi(x,t)|^2 + V(x)\right)\Psi(x,t), \tag{7}$$

$$\Psi(x,t) = e^{-i\mu t}\psi(x), \tag{8}$$

$$-\frac{1}{2}m\frac{d^2\psi(x)}{dx^2} + c|\psi(x)|^2\psi(x) + V(x)\psi(x) = \mu\psi(x), \tag{9}$$

$$\int_0^1|\psi(x)|^2dx = \int_0^1\rho(x)dx = 1, \tag{10}$$

in which the spatial coordinate x is scaled by the period d, the wave functions $\Psi(x, t)$ and $\psi(x)$ by $\sqrt{n_0}$, the periodic potential $V(x)$ and the chemical potential μ by $md^2/\hbar^2$, the potential strength v by $md/\hbar^2$, the time t by $\hbar/md^2$, and the nonlinear coefficient c by $n_0md^2/\hbar^2$.

We are interested in Bloch wave stationary solutions of the form

$$\psi(x) = e^{ikx}\phi_k(x), \tag{11}$$

where k is the Bloch wave number and $\phi_k(x)$ has the same period as the external potential $V(x)$.

A full set of Bloch wave solutions for a BEC in the Kronig–Penney potential can be found by decomposing the wave function $\psi(x)$ into density and phase:

$$\psi(x) = \sqrt{\rho(x)}e^{i\theta(x)}, \tag{12}$$

where the density function $\rho(x)$ is nonnegative and the phase function $\theta(x)$ is real. As shown in Eq. (6), the Kronig–Penney potential $V(x)$ is nonzero only when x is an integer. In the region $0 < x < 1$, therefore, the wave

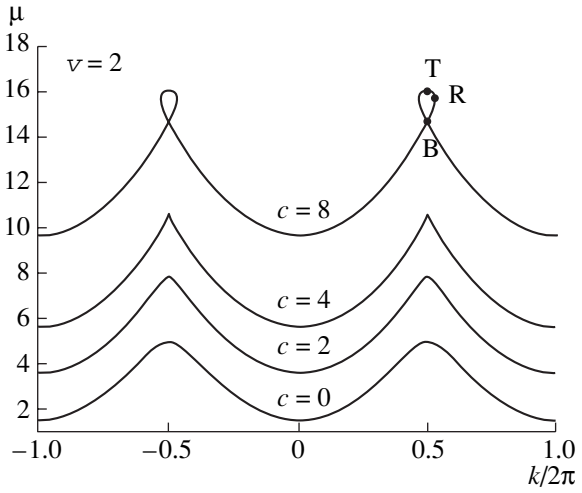

Fig. 1. Lowest Bloch bands at $v = 2$ for $c = 0$, 2, 4, and 8. As the nonlinear coefficient c increases, the Bloch band is vertically shifted higher and its tip becomes sharper. When the atomic interaction becomes sufficiently strong ($c > 2v$), a loop appears at the edge of the Brillouin zone.

function $\psi(x)$ is subject to the time-independent GP Eq. (9) without the presence of an external potential

$$-\frac{1}{2}\frac{d^2\psi(x)}{dx^2} + c|\psi(x)|^2\psi(x) = \mu\psi(x), \quad 0 < x < 1. \tag{13}$$

Inserting Eq. (12) into Eq. (13), we may finally arrive at the most general form of the solution in the case of no external potential:

$$\rho(x) = B + \frac{mb^2}{c}\mathrm{sn}^2(bx + x_0|m), \quad 0 < x < 1, \tag{14}$$

$$\theta(x) = \alpha\int_0^x \frac{dx}{\rho(x)}, \quad 0 < x < 1, \tag{15}$$

where sn is one of the twelve Jacobi elliptic functions and m, whose range is restricted within [0, 1], denotes not the atomic mass but the elliptic parameter. In this general solution, the free variables are the elliptic parameter m, the translational scaling b, the translational offset x_0, and the density offset B, while the phase prefactor α and the chemical potential μ are given as their functions

$$\alpha^2 = B\left(\frac{mb^2}{c} + B\right)(b^2 + Bc), \tag{16}$$

$$\mu = \frac{1}{2}(b^2(1 + m) + 3Bc). \tag{17}$$

A brief discussion of the derivation of Eqs. (14)–(17) can be found in [27].

We have hitherto ignored the Bloch wave condition (11). Assuming that the solution given in Eqs. (14) and (15) is but a segment of a Bloch wave stationary solution of the GP equation with the Kronig–Penney potential, we get the Bloch wave solution by extending the wave function $\psi(x)$, which has been restricted within (0, 1), onto the whole x axis according to

$$\psi(x + n) = e^{ikn}\psi(x), \quad n \in \mathbb{Z}, \tag{18}$$

which is a straightforward corollary of the Bloch wave condition (11). Equation (13) also gives the Bloch wave number

$$k = \theta(1) = \alpha\int_0^1 \frac{dx}{\rho(x)}, \tag{19}$$

which is functionally dependent on the four free variables. The effect of the Kronig–Penney potential (6) is to induce the boundary conditions

$$\lim_{\epsilon \to 0^+}(\rho(n + \epsilon) - \rho(n - \epsilon)) = 0, \tag{20}$$

$$\lim_{\epsilon \to 0^+}(\rho'(n + \epsilon) - \rho'(n - \epsilon)) = 4v\rho(n), \tag{21}$$

where n is an integer. Combining the boundary conditions with the normalization condition (10) of the wave function, we reduce the number of free variables from four to one and therefore determine the full set of Bloch wave solutions for a BEC in the Kronig–Penney potential, from which we are able to further compute the chemical potential μ and the Bloch wave number k by applying Eqs. (17) and (19), respectively. The set of chemical potentials $\mu(k)$ as a function of the Bloch wave number then forms the Bloch bands.

As the nonlinear coefficient c is positive in most experiments, reflecting the fact that the interactions between the BEC atoms are in most cases repulsive rather than attractive, we only compute the Bloch wave solutions of $c \geq 0$. We seek to find out how the Bloch bands change as the nonlinear coefficient c increases, i.e., as the atomic interaction becomes stronger, at a fixed potential strength v. The lowest and the second lowest Bloch bands for several different c at a fixed v are presented in Figs. 1 and 2, respectively.

We find that the structure of the Bloch bands is strongly dependent on the strength of the atomic interaction. The nonlinear bands are vertically shifted higher as compared with the linear (noninteracting) case of $c = 0$.

The deviation from the linear band structure grows as the nonlinear coefficient c increases. When the interaction between the BEC atoms is sufficiently strong, the band structure becomes quite different, marked by the emergence of loops at the edge or the center of the Brillouin zone. It is shown in our numerical results that the critical interaction strength for the onset of the loops, i.e., the minimum nonlinear coefficient for which

the loops appear in the Bloch bands, is twice the potential strength v no matter which band is being considered, the lowest or the higher ones.

3. LANDAU AND DYNAMICAL INSTABILITIES

The study of the stability of the Bloch states for a BEC in the presence of a periodic potential is essential. There are two types of instabilities: the Landau instability or energetic instability, for which certain small perturbations can lower the energy of the BEC system, and the dynamical instability, for which certain small deviations from the initial state grow exponentially in the course of time evolution.

3.1. Superfluidity and Landau Instability

Landau instability is often discussed along with a very remarkable property of quantum Bose liquids or gases known as superfluidity, i.e., the ability of a liquid or gas to flow without friction through capillaries or other types of tight spaces if its speed is below a critical value. For this interesting phenomenon, Landau proposed a simple explanation that a quantum current suffers viscosity only when the creation of the elementary excitations (phonons) of the system can lower its energy, in which case we say that the system suffers Landau instability and the superfluidity is therefore lost.

The same is true for a BEC in the presence of a periodic potential. If a BEC Bloch state remains in a local energy minimum against all sorts of small perturbations that break the periodicity of the system, the BEC flow is a superflow and suffers no viscosity. Otherwise, i.e., if certain small perturbations can lower the energy of the system, the state is an energy saddle point and the flow suffers Landau instability.

In order to determine whether small perturbations lower the energy of a given Bloch state, we apply to it a small perturbation

$$\psi'(x) = e^{ikx}(\phi_k(x) + \delta\phi_k(x)). \quad (22)$$

As a result of the periodicity of the BEC system, the perturbation $\delta\phi_k(x)$ can be decomposed into different modes $e^{\pm iqx}$:

$$\delta\phi_k(x) = u_k(x, q)e^{iqx} + v_k^*(x, q)e^{-iqx}, \quad (23)$$

where q is also a kind of Bloch wave number which labels the perturbation mode and ranges from $-\pi$ to π, and the perturbation functions $u_k(x, q)$ and $v_k(x, q)$ have the same period in x as the BEC system. Substituting the perturbed state (22) into the grand canonical Hamiltonian

$$\mathcal{H} = \int dx\left\{\psi^*\left(-\frac{1}{2}\frac{d^2}{dx^2} + V(x)\right)\psi + \frac{c}{2}|\psi|^4 - \mu|\psi|^2\right\} \quad (24)$$

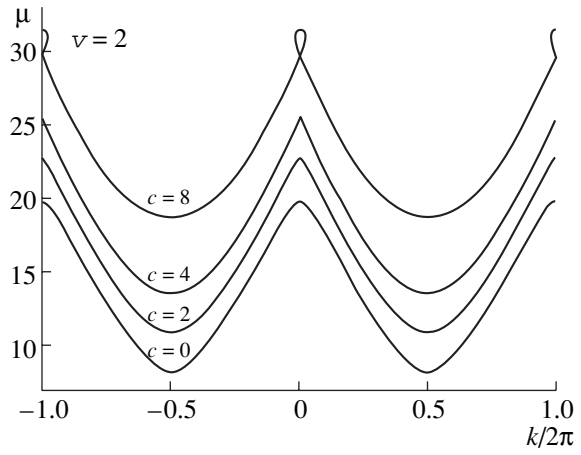

Fig. 2. Second lowest Bloch bands at $v = 2$ for $c = 0$, 2, 4, and $c = 8$. When the atomic interaction becomes sufficiently strong ($c > 2v$), a loop appears at the center of the Brillouin zone.

and neglecting terms of orders higher than two, we find the criterion on the Landau instability, that the Bloch wave $\phi_k(x)$ is a local energy minimum and therefore energetically stable if the operator

$$M_k(q) = \begin{pmatrix} \mathcal{L}(k+q) & c\phi_k^2 \\ c\phi_k^{*2} & \mathcal{L}(-k+q) \end{pmatrix} \quad (25)$$

with $\mathcal{L}(k')$ defined as

$$\mathcal{L}(k') = -\frac{1}{2}\left(\frac{d}{dx} + ik'\right)^2 + V(x) + 2c|\phi_k|^2 - \mu \quad (26)$$

is positive definite for all $-\pi \le q \le \pi$. Therefore, the Landau instability of the Bloch state $\phi_k(x)$ is determined by the eigenvalues $\lambda_k(q)$ of the operator $M_k(q)$.

We resort to numerical calculations to examine whether the operator $M_k(q)$ is positive-definite and whether the corresponding Bloch state is energetically stable. The numerical method employed in our case of the Kronig–Penney potential is the so-called method of discretization as opposed to the method of Fourier expansion, which is used to compute the instabilities of the BEC Bloch states in the sinusoidal potential. The method of discretization is elaborated in Appendix A in detail.

Our attention is focused on the Bloch states in the lowest Bloch band, including the loop if it appears. The results are summarized in the stability phase diagrams shown in the panels of Fig. 3, where a wide range of values of v and c are considered so as to exhibit how the instabilities change with the two system parameters. As the results have reflection symmetry in k and q, we only show the parameter region where they are both positive.

In the shaded (whether light or dark) area of each panel of Fig. 3, the operator $M_k(q)$ has one or more neg-

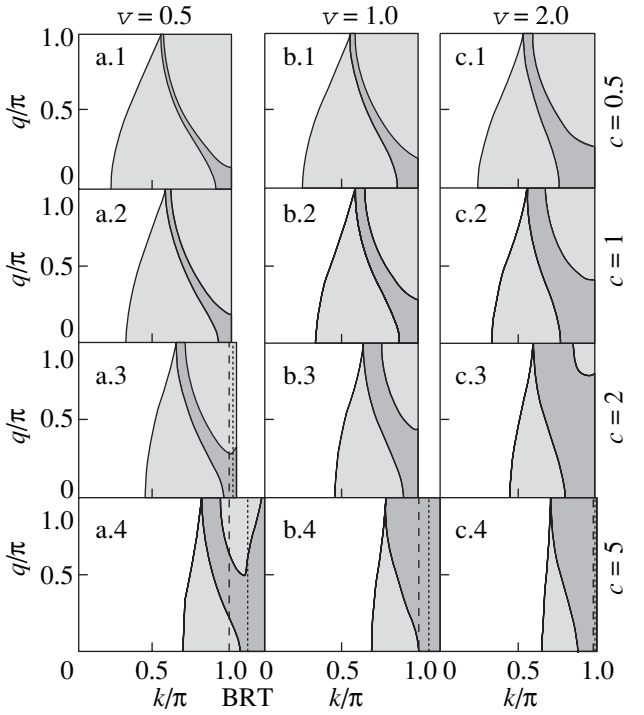

Fig. 3. Stability phase diagrams of Bloch states of a BEC in the Kronig–Penney potential. k is the wave number of the Bloch state and q is the wave number of the perturbation mode. In the shaded (whether light or dark) area, at least one of the excitation energies of the perturbation mode is negative. In the dark shaded area, the perturbation grows exponentially in the course of time evolution.

ative eigenvalues, rendering the corresponding Bloch state $\phi_k(x)$ energetically unstable. If, for a given value of k, none of the points (k, q) is in the shaded area, i.e., the vertical line at this k lies completely within the nonshaded area, then the corresponding Bloch wave $\phi_k(x)$ is a local energy minimum and represents a superflow. In this sense, the nonshaded area is also called the superflow region.

For panels (a.1–a.2), (b.1–b.3), and (c.1–c.3) of Fig. 3, there are no loops appearing in the Bloch bands. Therefore, the parameter region for these panels is $0 \le k \le \pi$ and $0 \le q \le \pi$. For the other four panels, i.e., (a.3–a.4), (b.4), and (c.4), loops do appear, and the range of k values is therefore enlarged. In each of these four panels, the long-dashed vertical line (––) represents the bottom of the loop, shown in Fig. 1 as point B at the edge of the Brillouin zone, the short-dashed vertical line (--) represents the rightmost edge of the loop, shown in Fig. 1 as point R, and the right border of the parameter region represents the top of the loop, shown in Fig. 1 as point T at the edge of the Brillouin zone. Therefore, the parameter region between the long-dashed line and the short-dashed line shows the instabilities of those Bloch states on the loop which are between point B and R, while the region between the short-dashed line and the right border shows the instabilities of the states between point R and point T. Note also that, in the latter region, the direction of the k axis is reversed beginning at the Bloch wave number of point R, which is greater than π, and ending at the Bloch wave number of the edge of the Brillouin zone which is exactly π. The instabilities of the Bloch states on the left half of the loop do not appear in the stability phase diagram, for they are represented by the right half as a result of the translation and reflection symmetry in the Bloch wave number k.

As we see in each column of Fig. 3, the phase boundary between the superflow region and the shaded area is strongly dependent on the nonlinear coefficient c. As the atomic interaction becomes stronger, the superflow region expands and the shaded area shrinks. The shaded area may even disappear from the parameter region when c becomes sufficiently large. On the other hand, the boundary does not depend very much on the potential strength v as can be seen in each row.

3.2. Dynamical Instability

Assume that a system experiences a small perturbation from its stationary state at a certain initial time. If in the course of time evolution the deviation remains bounded, we say that the state is dynamically stable. Otherwise, i.e., if the deviation grows exponentially with increasing time t, we say that the state is dynamically unstable or chaotic.

The dynamical instability of a BEC Bloch state in the Kronig–Penney potential can be determined from the linear stability analysis of the time-dependent GP Eq. (7). Assume that the Bloch state $\phi_k(x)$ is slightly perturbed at an initial time t_0

$$\Psi'(x, t) = e^{-i\mu t + ikx}(\phi_k(x) + \delta\phi_k(x, t)), \quad t \ge t_0, \quad (27)$$

where, similarly, the deviation $\delta\phi_k(x, t)$ can be decomposed into different modes $e^{\pm iqx}$

$$\delta\phi_k(x, t) = u_k(x, q, t)e^{iqx} + v_k^*(x, q, t)e^{-iqx}, \quad (28)$$

where q is the wave number of the perturbation mode and the perturbation functions $u_k(x, q, t)$ and $v_k(x, q, t)$ are periodic in x. Substituting the perturbed wave function (27) into the time-dependent GP Eq. (7) and keeping only the linear terms, we arrive at a linear differential equation describing the dynamical evolution of the perturbation function $u_k(x, q, t)$ and $v_k(x, q, t)$:

$$i\frac{\partial}{\partial t}\begin{pmatrix} u_k \\ v_k \end{pmatrix} = \sigma_z M_k(q)\begin{pmatrix} u_k \\ v_k \end{pmatrix}, \quad (29)$$

where $M_k(q)$ is the same operator as defined in Eq. (25) and

$$\sigma_z = \begin{pmatrix} 1 & 0 \\ 0 & -1 \end{pmatrix}. \quad (30)$$

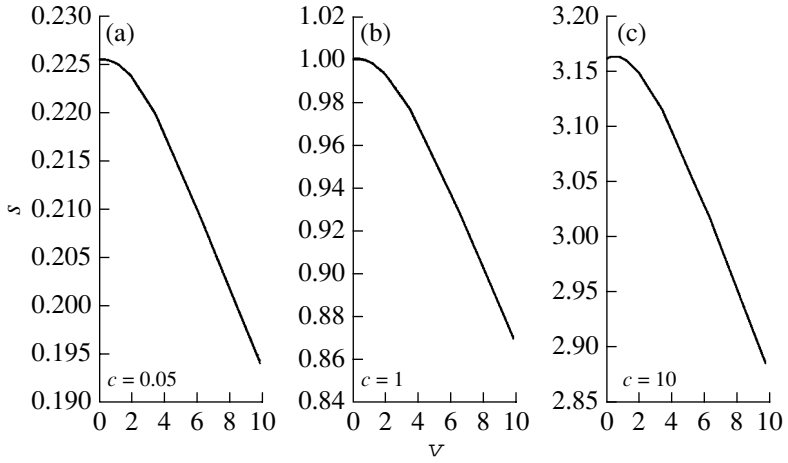

Fig. 4. Sound speed s of a BEC in the one-dimensional Kronig–Penney potential as a function of the potential strength v.

From Eq. (29), we know that the dynamical instability of the Bloch state $\phi_k(x)$ is determined by the eigenvalues $\varepsilon_k(q)$ of the operator $\sigma_z M_k(q)$. If its eigenvalues are all real for any $-\pi \le q \le \pi$, the Bloch state is dynamically stable. Otherwise, i.e., if the operator $\sigma_z M_k(q)$ has one or more complex eigenvalues for some value of q, the state suffers dynamical instability.

The dynamical instability of the Bloch states in the Kronig–Penney potential are also determined by numerical calculations and summarized in the stability phase diagrams of Fig. 3. Again the method of discretization is used.

In the dark shaded area of each panel of Fig. 3, at least one of the eigenvalues of the operator $\sigma_z M_k(q)$ is complex, rendering the corresponding Bloch state $\phi_k(x)$ dynamically unstable. If the vertical line at a give value of k stays completely out of the dark shaded area, the state is dynamically stable. Note that the dark shaded area lies completely inside the light shaded area, for it can be shown that the operator $M_k(q)$ cannot be positive-definite if the operator $\sigma_z M_k(q)$ has one or more complex eigenvalues [10].

The dark shaded area is strongly dependent on both the strength of the atomic interaction and the strength of the periodic potential. The dark shaded area recedes toward the right border of the parameter region with increasing nonlinear coefficient c and widens with increasing potential strength v.

4. SPEED OF SOUND

It is worth noting that the operator $\sigma_z M_k(q)$ also appears in the traditional Bogoliubov approach and its eigenvalues $\varepsilon_k(q)$ are just the spectrum of Bogoliubov excitations. It is well known that the Bogoliubov excitation at the long-wavelength limit is phonon-like. In other words, the excitation energy $\varepsilon_k(q)$ is linear in q in the limit $|q| \longrightarrow 0$. Of course, all these are true only when k is sufficiently small. As shown in Fig. 3 the excitation energy $\varepsilon_k(q)$ can be negative or even imaginary when k is large enough.

For the ground state of the system, which is at $k = 0$, the slope of the excitation energy $\varepsilon_k(q)$ in the long-wavelength limit is the speed of sound of the system. Namely, the speed of sound s of the system can be defined as

$$s = \lim_{q \to 0^+} \frac{d\varepsilon_0(q)}{dq} = \lim_{q \to 0^+} \frac{\varepsilon_0(q)}{q}. \tag{31}$$

We investigate how the sound speed varies in response to the changes of the strength of the atomic interaction or of the periodic potential. In particular, we are interested in the functional relationship between the sound speed s and the potential strength v for a given nonlinear coefficient c and how their relationship varies for different values of c. These dependences are shown in Fig. 4 by our numerical calculations.

As we see in Fig. 4, the sound speed of a BEC in the Kronig–Penney potential always falls monotonically with increasing potential strength, no matter whether the interaction between the BEC atoms is weak or strong. This is also the case for the sound speed in the one-dimensional sinusoidal optical lattice [28]. The same trend in these two different potentials reflects our general conclusion that, in any one-dimensional periodic potential, the speed of sound s as a function of the potential strength v has a vanishing slope and a negative second derivative at $v = 0$. This conclusion is based on an analytic expression of the sound speed in the weak potential limit of an arbitrary potential, which we find in [29]. In the case of the one-dimensional Kronig–Penney potential, the analytic expression becomes

$$s = \sqrt{c}\left(1 - v^2 \sum_{n=1}^{\infty} \frac{c}{(c + n^2\pi^2)^3} + \ldots\right), \tag{32}$$

which is in accurate accordance with the sound speed graphs in Fig. 4.

5. SUMMARY AND DISCUSSION

We have studied the instabilities and the sound speed of a BEC in the Kronig–Penney potential. The full set of Bloch-wave stationary solutions has been analyzed. We have investigated the Landau instability and dynamical instability of the Bloch states in the lowest Bloch band, including the loop if it appears. It has been shown that the stability phase diagram in the case of the Kronig–Penney potential is very similar to the sinusoidal case. We have also computed the speed of sound as a function of the strength of the one-dimensional Kronig–Penney potential. Our numerical calculation shows that, as the potential strength increases, the sound speed always falls monotonically, no matter whether the interaction between the BEC atoms is weak or strong. On the other hand, we have found an analytic formula which describes the functional relationship between the sound speed and the potential strength in the weak potential limit. Our numerical and analytical results are in accurate accordance.

APPENDIX A

METHOD OF DISCRETIZATION

If we use the method of Fourier expansion to compute the eigenvalues of the operators $M_k(q)$ and $\sigma_z M_k(q)$ numerically, we would have to set a cutoff in the Fourier series. However, the cutoff works poorly and incurs great numerical errors in the case of the Kronig–Penney potential. The method of discretization is therefore employed to replace the method of Fourier expansion in this case.

Our goal is to find an equivalent matrix for the operator $M_k(q)$ or $\sigma_z M_k(q)$. First, any continuous function $f(x)$ with period 1, such as the Bloch wave $\phi_k(x)$ or the density function $\rho(x)$, is discretized into an $N \times N$ diagonal matrix

$$\mathcal{M}(f) = \begin{pmatrix} f(0) & 0 & 0 & \dots & 0 \\ 0 & f\left(\frac{1}{N}\right) & 0 & \dots & 0 \\ 0 & 0 & f\left(\frac{2}{N}\right) & \dots & 0 \\ \vdots & \vdots & \vdots & \ddots & \vdots \\ 0 & 0 & 0 & \dots & f\left(\frac{N-1}{N}\right) \end{pmatrix}. \quad \text{(A1)}$$

Any constant C such as the chemical potential μ, being a special periodic function, is also represented by an $N \times N$ diagonal matrix

$$\mathcal{M}(C) = \begin{pmatrix} C & 0 & 0 & \dots & 0 \\ 0 & C & 0 & \dots & 0 \\ 0 & 0 & C & \dots & 0 \\ \vdots & \vdots & \vdots & \ddots & \vdots \\ 0 & 0 & 0 & \dots & C \end{pmatrix}. \quad \text{(A2)}$$

The matrix representation of the Kronig–Penney potential $V(x)$ cannot be given by Eq. (A1) owing to the discontinuity of the delta functions. Instead, the potential $V(x)$ is discretized into

$$\mathcal{M}(V) = v\begin{pmatrix} N & 0 & 0 & \dots & 0 \\ 0 & 0 & 0 & \dots & 0 \\ 0 & 0 & 0 & \dots & 0 \\ \vdots & \vdots & \vdots & \ddots & \vdots \\ 0 & 0 & 0 & \dots & 0 \end{pmatrix}. \quad \text{(A3)}$$

It remains to discretize the derivative operators d/dx and d^2/dx^2. Their matrix representations are

$$M\left(\frac{d}{dx}\right) = \frac{N}{2}\begin{pmatrix} 0 & 1 & 0 & \dots & -1 \\ -1 & 0 & 1 & \dots & 0 \\ 0 & -1 & 0 & \dots & 0 \\ \vdots & \vdots & \vdots & \ddots & \vdots \\ 1 & 0 & 0 & \dots & 0 \end{pmatrix} \quad \text{(A4)}$$

for the first-derivative operator and

$$\mathcal{M}\left(\frac{d^2}{dx^2}\right) = N^2\begin{pmatrix} -2 & 1 & 0 & \dots & 1 \\ 1 & -2 & 1 & \dots & 0 \\ 0 & 1 & -2 & \dots & 0 \\ \vdots & \vdots & \vdots & \ddots & \vdots \\ 1 & 0 & 0 & \dots & -2 \end{pmatrix} \quad \text{(A5)}$$

for the second-derivative operator. It is worth noting that our discretization keeps the anti-Hermitian property of the first-derivative operator d/dx and the Hermitian property of the second-derivative operator d^2/dx^2.

By applying Eqs. (A1)–(A5), we are able to write the operator $M_k(q)$ or $\sigma_z M_k(q)$ as a $2N \times 2N$ matrix and to compute the eigenvalues of the matrix numerically. The stability phase diagrams in Fig. 3 are plotted according to the numerical results obtained when N takes the value of 200.

ACKNOWLEDGMENTS

This work is supported by the "BaiRen" program of the Chinese Academy of Sciences, NSF of China (10504040), and the 973 project of China (2005CB724500).

REFERENCES

1. M. H. Anderson, J. R. Ensher, M. R. Matthews, et al., Science **269**, 198 (1995).
2. K. B. Davis, M.-O. Mewes, M. R. Andrews, et al., Phys. Rev. Lett. **75**, 3969 (1995).
3. C. C. Bradley, C. A. Sackett, J. J. Tollett, and R. G. Hulet, Phys. Rev. Lett. **75**, 1687 (1995).
4. J. C. Bronski, L. D. Carr, B. Deconinck, and J. N. Kutz, Phys. Rev. Lett. **86**, 1402 (2001).
5. J. C. Bronski, L. D. Carr, B. Deconinck, et al., Phys. Rev. E **63**, 036612 (2001).
6. S. Burger, F. S. Cataliotti, C. Fort, et al., Phys. Rev. Lett. **86**, 4447 (2001).
7. Biao Wu and Qian Niu, Phys. Rev. A **64**, 061603 (2001).
8. Biao Wu, R. B. Diener, and Qian Niu, Phys. Rev. A **65**, 025601 (2002).
9. A. Smerzi, A. Trombettoni, P. G. Kevrekidis, and A. R. Bishop, Phys. Rev. Lett. **89**, 170402 (2002).
10. Biao Wu and Qian Niu, New J. Phys. **5**, 104 (2003).
11. Y. Zheng, M. Kostrum, and J. Javanainen, Phys. Rev. Lett. **93**, 230401 (2004).
12. B. P. Anderson and M. A. Kasevich, Science **282**, 1686 (1998).
13. F. S. Cataliotti, S. Burger, C. Fort, et al., Science **293**, 843 (2001).
14. Dae-II Choi and Qian Niu, Phys. Rev. Lett. **82**, 2022 (1999).
15. Biao Wu and Qian Niu, Phys. Res. A **61**, 023402 (2000).
16. O. Zobay and B. M. Garraway, Phys. Rev. A **61**, 033603 (2000).
17. O. Morsch, J. H. Müller, M. Cristiani, et al., Phys. Rev. Lett. **87**, 140402 (2001).
18. M. Cristiani, O. Morsch, J. H. Müller, et al., Phys. Rev. A **65**, 063612 (2002).
19. G. Ritt, C. Geckeler, T. Salger, G. Cennini, and M. Weitz, cond-mat/0512018 (2006).
20. E. P. Gross, Nuovo Cimento **20**, 454 (1961).
21. L. P. Pitaevskii, Zh. Eksp. Teor. Fiz. **40**, 646 (1961) [Sov. Phys. JETP **13**, 451 (1961)].
22. B. T. Seaman, L. D. Carr, and M. J. Holland, Phys. Rev. A **71**, 033622 (2005).
23. P. E. Moskowitz, P. L. Gould, and S. R. Atlas, Phys. Rev. A **71**, 033609 (2005); D. E. Pritchard, Phys. Rev. Lett. **51**, 370 (1983).
24. I. Danshita, S. Kurihara, and S. Tsuchiya, Phys. Rev. A (1998); M. Kramer, C. Menotti, and L. Pitaevskii **72**, 053611 (2005); I. Danshita and S. Tsuchiya, cond-mat/0607195.
25. P. L. Gould, G. A. Ruff, and D. E. Arid, Phys. Rev. A **70**, 023609 (2004).
26. C. Salomon, J. Dalibard, A. Aspect, et al., Phys. Rev. Lett. **59**, 1659 (1986).
27. B. T. Seaman, L. D. Carr, and M. J. Holland, Phys. Rev. A **71**, 033609 (2005).
28. K. Berg-Sorensen and K. Molmer, Phys. Rev. A **58**, 1480 (1998); M. Kramer, C. Menotti, L. Pitaevskii, and S. Stringari, Eur. Phys. J. D **27**, 247 (2003).
29. Z. X. Liang, Xi Dong, Z. D. Zhang, and Biao Wu (in preparation).